Optik - International Journal for Light and Electron Optics 273 (2023) 170423

Contents lists available at ScienceDirect

Optik

journal homepage: www.elsevier.com/locate/ijleo

Theoretical analysis on improving output power of continuous-wave single-wavelength two-photon pumped Rb-vapor laser with mid-infrared seed laser

Yanhui Ji [a,b], Yang He [a,*], Li Pan [a,b], Jiamin Wang [a,b], Fei Chen [a]

[a] State Key Laboratory of Laser Interaction with Matter, Changchun Institute of Optics, Fine Mechanics and Physics, Chinese Academy of Sciences, 3888 Dongnanhu Road, Changchun, Jilin 130033, China
[b] University of Chinese Academy of Sciences, Beijing 100049, China

ARTICLE INFO

Keywords:
Two-photon absorption
Alkali vapor laser
Blue laser
Mid-infrared laser
Mid-infrared seed laser

ABSTRACT

We theoretically prove that introducing 5.23-μm mid-infrared (MIR) seed laser can greatly increase output power of two-photon pumped Rb-vapor laser (Rb-TPAL) for the first time. Firstly, MIR laser stimulated radiation is added to the three-dimensional calculation model we reported in Ref. [1]. Then we simulate the Rb-TPAL pumped by a high-power continuous-wave laser diode and analyze the effects of MIR seed power and direction, vapor cell temperature and length, waist radii of pump and MIR seed, and output mirror reflectance on the output characteristics. The results show that by optimizing the above parameters, the MIR seed laser can not only significantly improve the output power and conversion efficiency of blue and MIR laser, but also reduce the pump and temperature thresholds of blue laser. This study can be useful for designing a TPAL system with high-power dual-waveband laser output.

1. Introduction

Alkali-vapor lasers are divided into single-photon pumped alkali lasers and two-photon pumped alkali vapor lasers (TPALs) according to the number of absorbed pump photons from the ground state to the pump upper states. Usually, alkali-vapor lasers absorb a near infrared photon through $n^2S_{1/2}$ to $n^2P_{3/2}$ transitions, and generate a near infrared photon through $n^2P_{1/2}$ to $n^2S_{1/2}$ transitions (n = 4 for K, n = 5 for Rb and n = 6 for Cs). Single-photon pumped K, Rb and Cs vapor laser can achieve single-wavelength laser output at 770 nm, 795 nm and 895 nm, respectively. With laser diodes (LDs) pumping, the single-photon pumped alkali laser have been scaled to kW levels [2–4]. Compared with the single-photon pumped alkali lasers, TPALs can output the multi-wavelength laser in visible, near-infrared, mid-infrared (MIR) and even far-infrared bands by absorbing two photons and pumping alkali atoms to higher states. One of their advantages is the realization of coaxial output of blue laser and MIR laser, which effectively avoid the dilemma of laser beam combining. The generated MIR and blue dual-band laser can be used in many fields, such as imaging, laser spectroscopy, underwater communication, and remote sensing surveys [5–8]. Another advantage is that no hydrocarbon gas is required as a buffer gas, and dual-wavelength laser output can be achieved without buffer gas or adding a small amount of He [9,10].

TPALs can be divided into dual-wavelength and single-wavelength excitation systems that use dual-wavelength or single-wavelength pump laser, respectively. The realization method of dual-wavelength excitation TPALs are complicated, which need to

* Corresponding author.
E-mail address: heyang_3g@126.com (Y. He).

https://doi.org/10.1016/j.ijleo.2022.170423
Received 27 September 2022; Received in revised form 12 December 2022; Accepted 12 December 2022
Available online 13 December 2022

adjust the polarization of the pump laser and combine the two pump beams. Single-wavelength excitation TPALs do not need any complex pump laser system or any complicated optical adjustment structure to meet the phase-matching condition; thus, a systematical study of single-wavelength excitation TPALs is very meaningful. In 1976, the transitions from $5^2S_{1/2}$ to $n^2D_{3/2}$ and $n^2D_{5/2}$ (n = 11–32) were found in Rb by single-wavelength two-photon pump for the first time [11]. However, due to the lack of suitable pump source and corresponding detection equipment, the achievements before 2010 mainly focused on the two-photon absorption characteristics, high-order nonlinear effect, frequency conversion characteristic, etc [12–14]. Recently, with the development of high-power narrow-linewidth laser technology and the increasing maturity of single-photon pumped alkali laser, single-wavelength excitation TPALs technology is rapidly developing. By improving the pump intensity and polarization, alkali vapor pressure, as well as temperature dependence, single-wavelength excitation Rb-vapor TPALs (Rb-TPALs) and Cs-vapor TPALs (Cs-TPALs) achieved blue laser output [10,15–18]. However, the output power and optical-optical efficiency of single-wavelength excited TPALs are very low, which limits the application of TPALs. For the blue laser, the highest optical-optical efficiency only achieved 1% in the Rb-TPAL pumped by a dye laser at 778.1 nm in 2016 [19]. The output power of blue laser can only reach mW level [20,21]. For the MIR laser, the window material of the alkali-vapor cell used in TPALs is mainly quartz or pyrex glass that has a strong absorption of MIR laser. Therefore, the power and efficiency of MIR laser generated by TPAL are extremely low [22–24], many TPALs system only achieve blue laser output without generating the MIR laser [20,21]. In terms of theory, we proposed the theoretical model of TPAL in [1] for the first time and analyze the reasons for the low power and efficiency of blue laser in Rb-TPALs. The simulation results suggest that a considerable number of Rb atoms will gather at $5^2D_{5/2}$ energy level if not consider MIR stimulated radiation. The spontaneous emission rate between $5^2D_{5/2}$ energy level and $6^2P_{3/2}$ energy level is relatively low, which makes it difficult for a large number of particles in the $5^2D_{5/2}$ level to transition to the $6^2P_{3/2}$ level resulting in low power and conversity efficiency of the blue laser.

To solve this problem, we propose that 5.23-μm MIR seed laser can be introduced to increase the transition rate from $5^2D_{5/2}$ to $6^2P_{3/2}$ in Rb-TPAL, which not only improves the output power and optical-optical efficiency of blue laser, but also amplifies the 5.23-μm MIR laser, a similar method was experimentally tested in Ref. [25]. Gai et al. found that introduce a MIR seed laser at 2.42 μm can enhance the intensity of the laser at 455.6 nm by promoting the transition process of Cs atoms from $7^2D_{5/2}$ to $7^2P_{3/2}$ in Cs-TPAL experiment. The experimental results show the feasibility of introducing 5.23-μm MIR seed laser into Rb-TPAL to increase output power and optical-optical efficiency of blue and MIR laser.

Against this backdrop, we theoretically verify the influence of MIR seed laser on output power and conversion efficiency of Rb-TPAL. Firstly, we establish a three-dimensional (3D) theoretical model of TPAL considering the MIR laser stimulated radiation base on the rate equations. And then we simulate the influence of MIR seed laser on the output characteristics of Rb-TPAL pumped by a high-power continuous-wave (CW) LD. We theoretically prove that the MIR seed laser can effectively improve the output power and conversion efficiency of Rb-TPAL for the first time. Then, we analyze the effects of MIR seed laser power and direction, vapor cell length and temperature, waist radii of pump and MIR seed, and output mirror reflectance on the characteristics of the blue and MIR laser. Thus, the model and simulation results will contribute to the design of high-power dual-wavebands TPAL systems.

2. Computation method

We report a 3D theoretical model considering the MIR laser stimulated radiation based on the rate equation. The model considers the configuration of a CW single-wavelength end-pump Rb-TPAL with seed laser at 5.23 μm. As shown in Fig. 1, the Rb-vapor cell is cylindrical with length L and diameter D. The laser and pump beams propagate along the z-axis, and the direction of the pump laser is positive. The pump laser is incident from the window A of the vapor cell and exits from the window B. The coordinate origin locates in

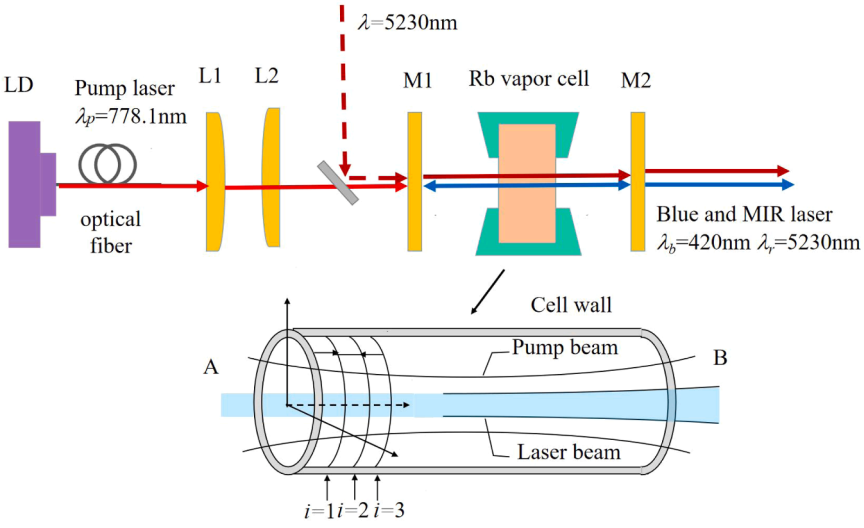

Fig. 1. Schematic diagram of single-wavelength excitation Rb-TPAL system.

the center of the cross-section, and the coordinate axes of the vapor cell cross-section are x and y. The pumping source is chosen as CW fiber-coupled LD at 778.1 nm. The pump, blue and MIR laser intensities are I_p, $I_b^{\pm}$ and $I_r^{\pm}$, respectively (+ and – indicate laser beams propagating in the $+z$ and $-z$ directions). The intensities of MIR seed laser, MIR output laser and blue output laser are I_{rin}, I_{rout}, and I_{bout}.

The mechanism of two-photon absorption and energy level transition process of Rb-TPAL are shown in Fig. 2. The Rb atoms are excited by absorbing two pump photons at 778.1 nm from the ground state $5^2S_{1/2}$ to the upper states $5^2D_{5/2}$ via the intermediate virtual level, which marked with the dotted line. Then 5.23-μm MIR photons are generated from the $5^2D_{5/2}$ to $6^2P_{3/2}$ transition. And the blue laser at 420 nm is produced due to the transition from the $6^2P_{3/2}$ energy level back to the ground state $5^2S_{1/2}$. When quartz or pyrex glass is used as window material, 5.23-μm MIR laser is difficult to oscillate due to the strong absorption of window. The spontaneous emission rate between $5^2D_{5/2}$ to $6^2P_{3/2}$ is relatively low that makes it difficult to cause a large number of particles from the $5^2D_{5/2}$ level to the $6^2P_{3/2}$ level, resulting in a lower output power of blue laser. Therefore, we propose a way to introduce the 5.23-μm MIR seed laser to Rb-TPAL. Even though the vapor cell window has a large absorption of MIR laser, partial MIR seed laser can still enter the vapor cell through the window. The transition rate from $5^2D_{5/2}$ to $6^2P_{3/2}$ can be increased by stimulated radiation of MIR laser, which not only increases the output power blue laser, but also obtains high-power MIR laser output.

According to the kinetic processes, we can obtain the rate equations that describe the population distributions of Rb-TPAL

$$\frac{dN_1}{dt} = \frac{-N_1\sigma_{13}I_p}{h\nu_p} + \frac{(N_2 - 2N_1)\sigma_{21}I_b}{h\nu_b} + \frac{N_3}{\tau_2} + \frac{N_2}{\tau_1},$$

$$\frac{dN_2}{dt} = \frac{(N_3 - 1.5N_2)\sigma_{32}I_r}{h\nu_r} - \frac{(N_2 - 2N_1)\sigma_{21}I_b}{h\nu_b} - \frac{N_2}{\tau_1} + \frac{N_3}{\tau_3},$$

$$N_1 + N_2 + N_3 = N_0 \tag{1}$$

where N_1, N_2, and N_3 are the densities at the levels ground level ($5^2S_{1/2}$), upper pump level ($6^2P_{3/2}$), and upper laser level ($5^2D_{5/2}$), respectively. h is the Planck's constant. ν_b, ν_p and ν_r are the central frequency of blue laser, pump laser and MIR laser, respectively. σ_{13}, σ_{21} and σ_{32} are the pump absorption cross section, blue laser emission cross section, and MIR laser emission cross section, respectively. τ_i (i = 1,2,and 3) is the radiative lifetime of upper level, calculated in [1].

N_0 is the total Rb atom population density, which strongly influenced by cell temperature T [26].

$$n_{tot} = 133.322 \times 102.881 + 4.312 - \frac{4040}{T} \Big/ kT \tag{2}$$

The g_{21} (x, y, z) and g_{21} (x, y, z) are the saturation gain coefficient of the blue laser and MIR laser at the position (x, y, z), respectively. σ (x, y, z) is saturation absorption coefficient. They can be written as:

$$g_{21}(x,y,z) = \sigma_{21}[N_2(x,y,z) - 2N_1(x,y,z)] \tag{3}$$

$$g_{32}\left(x,y,z\right) = \sigma_{32}\left[N_3(x,y,z) - \frac{3}{2}N_2\left(x,y,z\right)\right] \tag{4}$$

$$\sigma(x,y,z) = \sigma_{13}N_1 = \sigma_{TAT}I_PN_1(x,y,z) \tag{5}$$

where σ_{TAP} is the two-photon absorption cross section (cm^4/W). Our group derived a calculation formula based on coupled wave equations [27]:

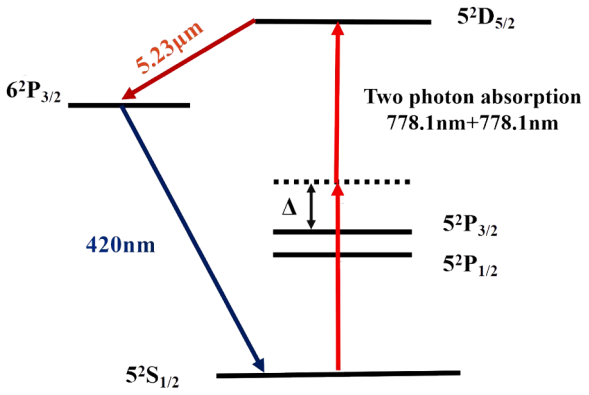

Fig. 2. Schematic illustration of energy structures and transition process of Rb-TPAL.

$$\sigma_{TPT} = \frac{3\cdot(2\pi\cdot\nu_P)^3}{k_p{}^2c^2N_0}\mu_0 \mathrm{Im}\left[\chi^{(3)}\left(-\nu_b,\nu_P,\nu_P,-\nu_r\right)\right]\times S_{FF''}\times f_{iso}\times f_F \tag{6}$$

Where k_p is pumping laser wave number, μ_0 is permeability of vacuum and c is the speed of light in vacuum. Im [$\chi^{(3)}$] is the imaginary part of third-order susceptibility of Rb in four-wave mixing process. The values of relative natural abundance $f_{iso}(Rb_{85})$ and $f_{iso}(Rb_{87})$ are 72.2% and 27.8%, respectively. $S_{FF''}$ is hyperfine line strengths and f_F is statistical distribution of population among F states of ground energy level.

The paraxial approximation can be used to simulate the propagation process of the blue and MIR laser in resonant cavity. In our study, the spatial distribution of the single-wavelength excitation Rb-TPAL laser intensity is calculated by beam propagation equation. In the free space part of the resonator, the paraxial wave equations for calculating the blue and MIR laser amplitude A_b and A_r are written as [28].

$$\begin{aligned} 2ik_b\frac{\partial A_b(x,y,z)}{\partial z} &= \frac{\partial^2 A_b(x,y,z)}{\partial x^2}+\frac{\partial^2 A_b(x,y,z)}{\partial y^2} \\ 2ik_r\frac{\partial A_r(x,y,z)}{\partial z} &= \frac{\partial^2 A_r(x,y,z)}{\partial x^2}+\frac{\partial^2 A_r(x,y,z)}{\partial y^2} \end{aligned} \tag{7}$$

Where k_b and k_r are the wave numbers of blue laser and MIR laser in vacuum, respectively. For the laser propagating in the vapor cell of the resonant cavity, the formulas for calculating the blue and MIR laser amplitude A_b and A_r are written as [28].

$$\begin{aligned} 2ik_b\frac{\partial A_b(x,y,z)}{\partial z} &= \frac{\partial^2 A_b(x,y,z)}{\partial x^2}+\frac{\partial^2 A_b(x,y,z)}{\partial y^2} \\ &\quad +ik_b g_{21}(x,y,z)A_b(x,y,z) \\ 2ik_p\frac{\partial A_p(x,y,z)}{\partial z} &= \frac{\partial^2 A_p(x,y,z)}{\partial x^2}+\frac{\partial^2 A_p(x,y,z)}{\partial y^2} \\ &\quad +ik_p\sigma(x,y,z)A_p(x,y,z) \end{aligned} \tag{8}$$

For absorbed pump beam in the alkali vapor cell, the pump amplitude A_p is calculated as

$$\begin{aligned} 2ik_p\frac{\partial A_p(x,y,z)}{\partial z} &= \frac{\partial^2 A_p(x,y,z)}{\partial x^2}+\frac{\partial^2 A_p(x,y,z)}{\partial y^2} \\ &\quad +ik_p\sigma(x,y,z)A_p(x,y,z) \end{aligned} \tag{9}$$

The blue and MIR laser in the Rb vapor cell and the free space inside the resonant cavity can be numerically calculated by solving Eqs. (1)–(8). An iterative method is proposed to numerically simulate the laser resonant in the cavity: The gain medium of Rb-TPAL is divided into small volume segments of length Δz along the z-axis of the Rb-vapor cell. The initial value of the pump intensity I_p (x, y, 0) and MIR seed laser intensity I_{rin} (x, y, 0) or I_{rin} (x, y, L) and is set by Gaussian functions. The blue laser intensity I_b (x, y, 0) is chosen arbitrarily. The initial value of MIR laser intensity I_r is determined by I_{rin}. In steady-state CW operation all the time derivatives in Eq. (1) are zero and the population densities N_1, N_2, and N_3 are determined, I_p (x, y, Δz), I_r (x, y, Δz) and I_b (x, y, Δz) are obtained by substituting Eqs. (3)–(6), and (8–9); I_b (x, y, Δz) = I_b^+ (x, y, Δz) + I_b^- (x, y, Δz) and I_r (x, y, Δz) = I_r^+ (x, y, Δz) + I_r^- (x, y, Δz) are calculated using the complex amplitudes stored in the previous step. The blue and MIR laser intensity free space part of the resonator can be calculated using Eq. (7). The dual-waveband laser is round-trip propagated through the cavity until the values of the pump and laser intensity stabilize. Accordingly, the intensity of the pump laser, MIR laser and blue laser of the Rb-TPAL is obtained. And then we can calculate the output power of blue laser P_{out} and MIR laser P_{rout}.

Table 1
Parameters used in the model.

Parameters	Definition	Value
σ_{32}	Stimulated emission cross section of MIR	2.367×10^{-11} cm^2
λ_r	MIR central wavelength	5.23 μm
NA	numerical aperture of the pump fiber	0.22
r_{fiber}	Pump core radius	200 μm
ω_p	Waist radius of pump laser	400 μm
ω_r	Waist radius of MIR seed laser	400 μm
P_p	Pump power	100 W
R_b	Output mirror M2 reflectivity of blue laser	15%
T_w	Vapor cell transmission of blue and MIR laser	95%
L	Vapor cell length	0.45 cm
T	Vapor cell temperature	220 ℃

3. Results and discussions

In this section, the simulation and optimization of a Rb-TPAL pumped by a high-power CW LD are conduction and explore the effect of MIR seed laser on the output characteristics of blue laser and MIR laser. The simulation conditions are as Table 1. The other parameters are the same as those in [1].

3.1. Influence of input power and direction of MIR seed laser

By our model, we simulate the influence of MIR seed laser on output characteristics of TPAL in four cases: co-direction, counter-direction, co- direction double-pass and counter- direction double-pass.

As shown in Fig. 3, M1 and M2 are input mirror and output mirror of the resonator respectively. Fig. 3(a) is the co-direction case: the MIR seed laser and pump laser are combined by a dichroic mirror (DM) co propagate into the resonator, M1 and M2 have high transmission for 5.23-μm MIR laser. The MIR laser and blue laser can output coaxially in the same direction. Fig. 3(b) shows the counter-direction case: the direction of MIR seed laser is reverse to the pump laser, and the MIR laser output in the counter direction of blue laser. The other parameters are consistent with the Fig. 3(a). Fig. 3(c) shows the co-direction double-pass case: after reflected by the polarized beam-splitter (PBS), the s-polarized MIR seed laser and pump laser are combined by the DM and co-propagating. M1 and M2 are antireflection-coated and high-reflection-coated at 5.23-μm, respectively. A quarter-wave plate (QWP) is added to the resonator, the angle between the fast axis of the QWP and the MIR seed polarization direction is 45°. The MIR laser is transmitted through M1 and reflected by M2, then converted into p-polarized MIR laser by pass through the vapor cell and QWP twice, finally outputs through M1, DM and PBS in the counter direction of blue laser. Fig. 3(d) shows the counter-direction double-pass case: the experimental setup is similar to Fig. 3(c), the difference is that M1 is high-reflection-coated at 5.23-μm, and M2 is antireflection-coated for MIR laser. The propagation direction of MIR seed laser is reverse to the pump laser, and MIR laser and blue laser output in the co-direction.

Fig. 4 shows the output power of the blue laser P_{bout} as a function of the input power of MIR seed laser P_{rin} under different cases. It can be seen that when $P_{rin} < 0.01$ W, P_{bout} increases with the increase of P_{rin}. When P_{rin} is 0 and 0.01 W, P_{bout} is ~0.4 W and ~6.6 W, respectively. This indicates that introduction of 5.23-μm MIR seed laser can significantly improve the output power of blue laser. At the same time, the way of introduction MIR seed laser has little effect on the output power of blue laser. However, when $P_{rin} > 0.01$ W, the output power of blue laser does not continue to increase and stabilize at ~6.6 W. Fig. 5 shows the distribution of population densities N_2 at $6^2P_{3/2}$ in co-direction case under $P_{rin} = 0$ W, 0.0001 W, 0.01 W and 0.1 W, respectively. It can be seen from Fig. 5(a-c), when $P_{rin} \leq 0.01$ W, N_2 increases as the increase of P_{rin} in the pump laser irradiation region, which indicates that the transition rate from $5^2D_{5/2}$ to $6^2P_{3/2}$ increases, thus promoting the output power of blue laser. However, when $P_{rin} > 0.01$ W, N_2 tends to be saturated as shown in Fig. 5(c-d). As a result, P_{bout} no longer increases and tends to be stable. Therefore, no matter how the MIR seed laser is introduced, when MIR seed power is large enough, the output power of blue laser will not continue to increase after reaching the maximum.

The results in Fig. 4 also show that P_{rin} affects the output power of MIR laser P_{rout}. Compared with the four cases in Fig. 3(a-d), P_{rout} grows with increase of P_{rin}. When P_{rin}= 1 W, P_{rout} in the four cases is 1.793 W, 1.872 W, 1.625 W and 1.794 W, respectively. However, when P_{rin} continues to increase, P_{rout} begins to be lower than P_{rin}. When P_{rin}= 10 W, P_{rout} in the four cases is 9.107 W, 10.043 W, 8.878 W and 9.008 W, respectively. This indicates that when the P_{rin} is too large, the MIR seed laser can not be amplified or even be absorbed. When 0.01 W < P_{rin} < 1 W, the MIR laser can be amplified and the output power blue laser reaches maximum. Therefore, we should choose the appropriate MIR seed laser power to obtain high-power and high-efficiency blue and MIR laser output in the TPAL

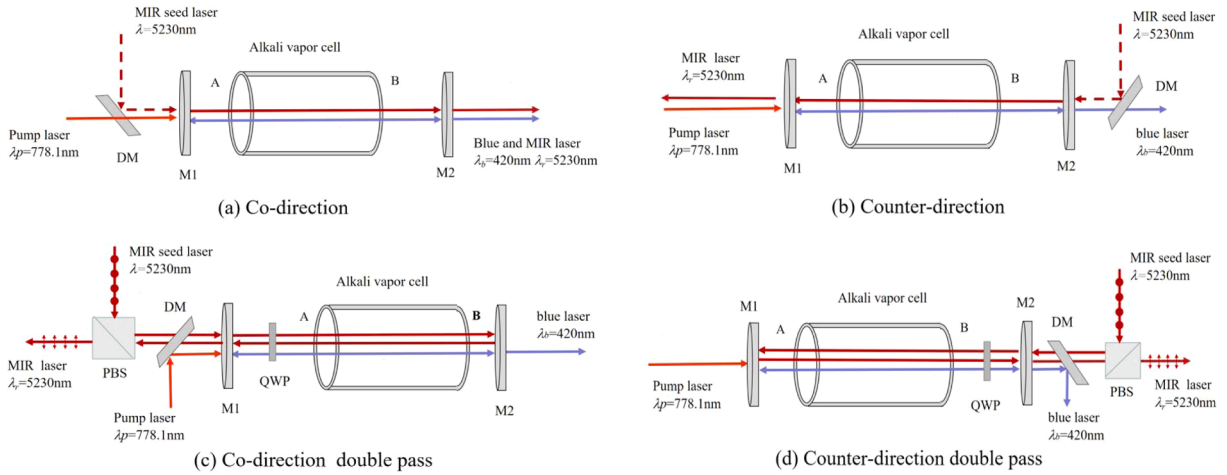

Fig. 3. Schematics of the TPAL under four cases of the introduction of MIR seed laser and pump laser in (a) co-direction (b)counter- direction (c)co-direction double pass (d) counter- direction double-pass. DM, dichroic mirror; QWP, quarter-wave plate; PBS, polarized beam-splitter; M1, input mirror; M2, output mirror.

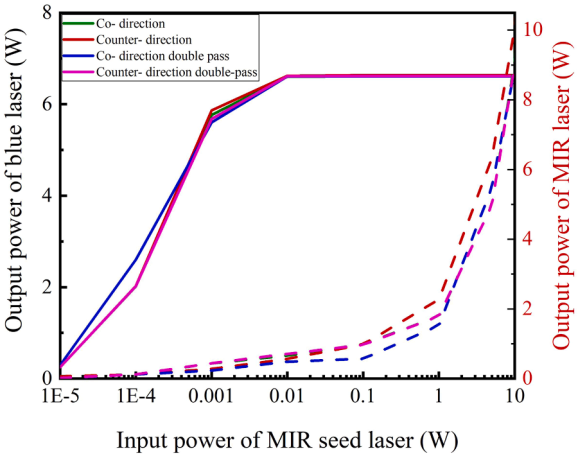

Fig. 4. The output power of the blue laser and MIR laser as a function of the input power of MIR seed laser. (Solid line is blue laser output power, the dotted line is MIR output power).

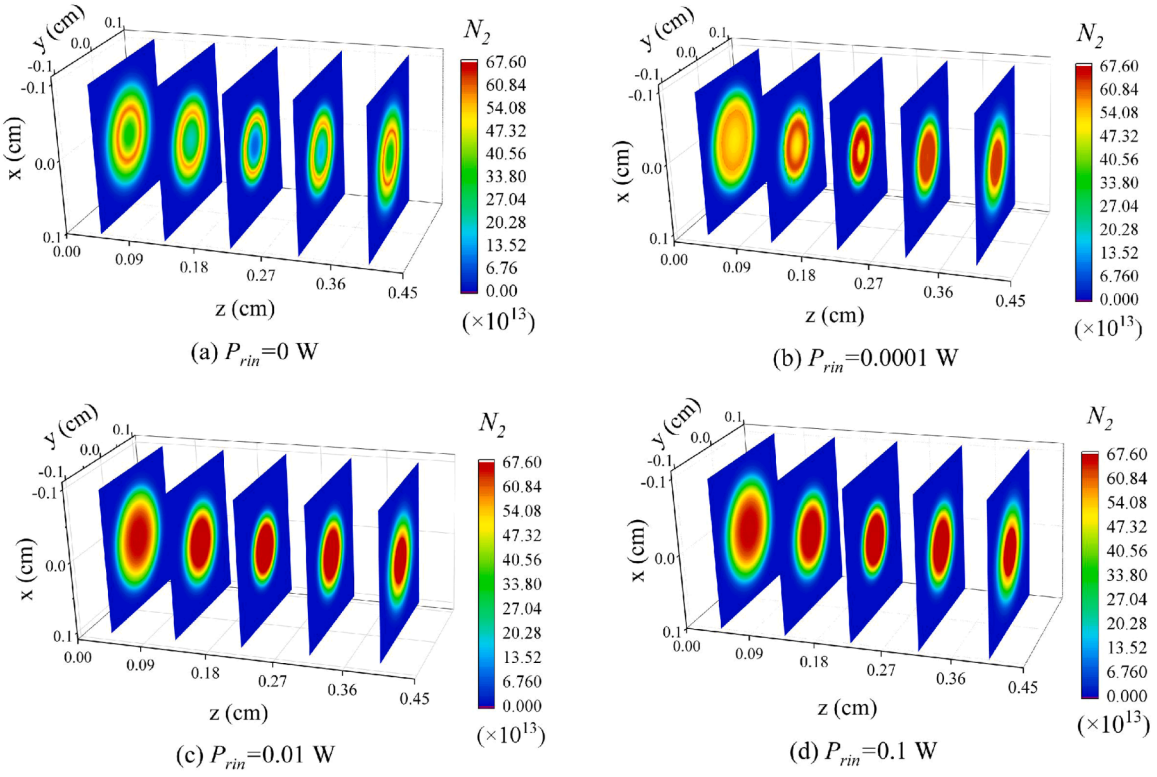

Fig. 5. Distribution of population densities of $6^2 P_{3/2}$ in the vapor cell at steady state under different P_{rin} in the co-direction case.

experiments. P_{rout} is the largest in the counter-direction case, and the other three cases are similar. Fig. 6 shows the distribution of gain coefficients of MIR laser when MIR laser is introduced in different directions when P_{rin}= 1 W. It can be seen that the MIR gain in Fig. 6 (b) reaches largest. Therefore, the MIR laser power in the counter-direction case is the highest.

Compared with the four cases, the values of P_{bout} are almost identical, and P_{rout} in the counter-direction case is the largest, but the value is little different from the other three cases. For the experimental setup of Rb-TPAL in the cases of counter-direction, counter-direction double-pass and co-direction double-pass, they are complex and difficult to realize. Although the output power of MIR laser in the counter-direction case is slightly larger than the co-direction case, the blue laser and MIR laser cannot output in the same direction. The experimental setup under the co-direction case is relatively simple, and the blue and MIR laser can output in the co-direction coaxially. Therefore, we only consider the co-direction case in the following simulation.

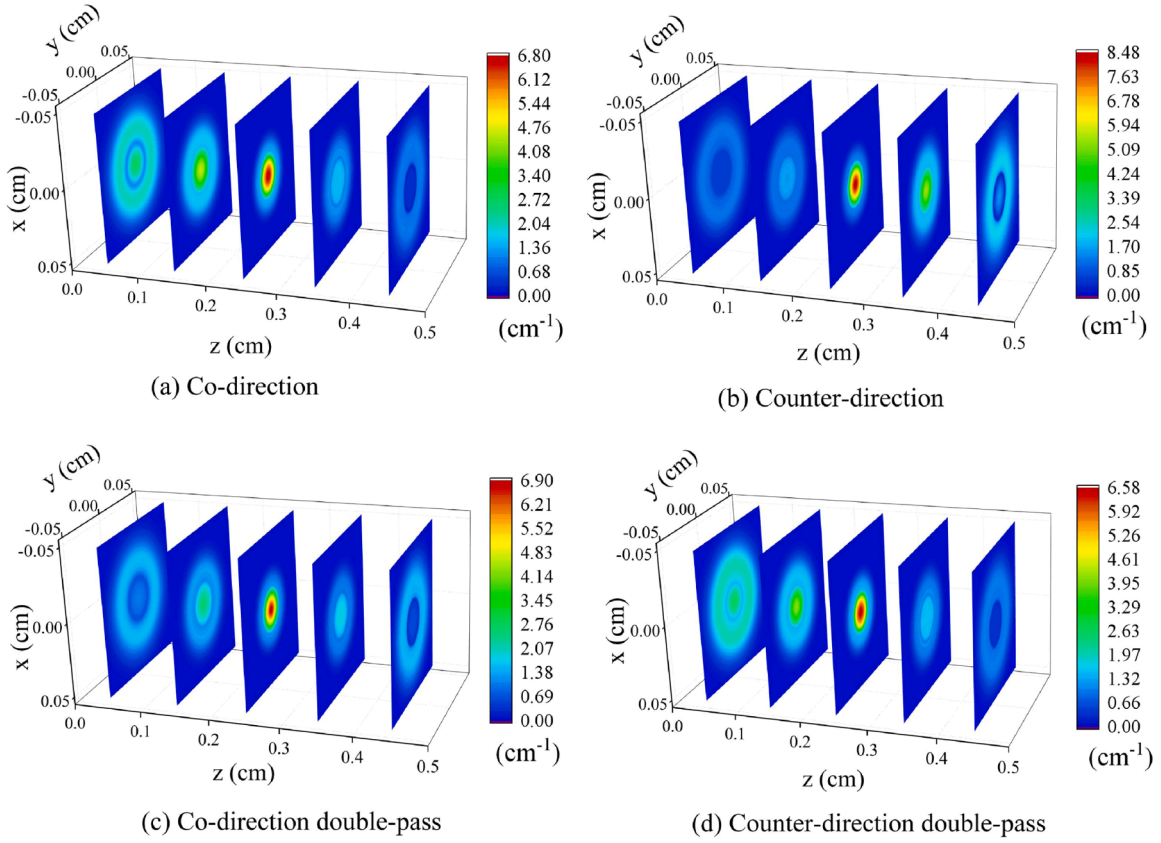

Fig. 6. Distribution of gain coefficients of MIR laser in the vapor cell at steady state when MIR laser is introduced in different directions when P_{rin}= 1 W.

3.2. *Temperature and length of Rb-vapor cell*

In order to obtain high power and high conversion efficiency of blue and MIR laser, P_{rin} is set to 1 W, and the other parameters are the same as mentioned above. We simulate the relationship between the output power of blue laser P_{bout} and MIR laser P_{rout} as a function of the cell length L at different temperatures T.

Fig. 7 displays the output power as a function of L at different T. There is no MIR seed laser in Fig. 7(a), and Fig. 7(b) shows the

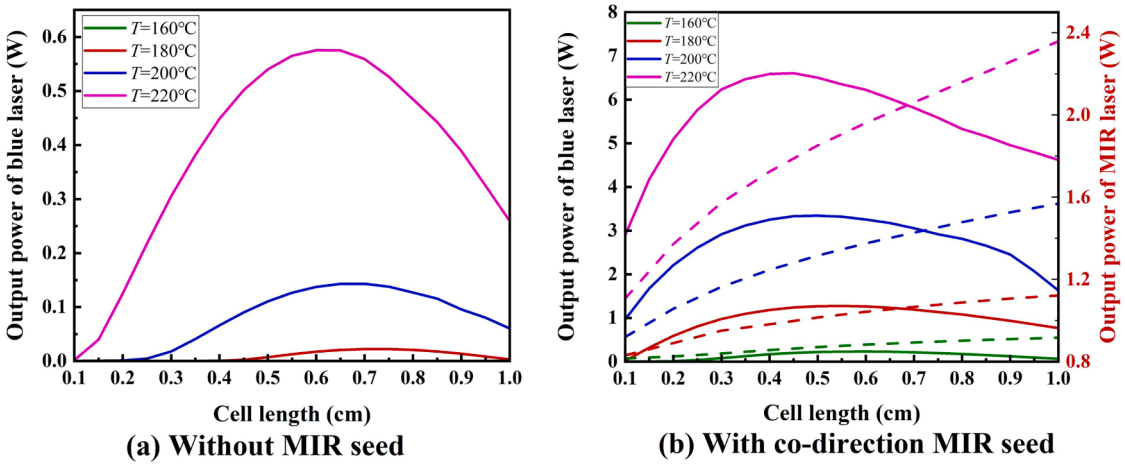

Fig. 7. Dependence of output power and cell length under different temperature conditions when P_{rin}= 1 W. (a) is without MIR seed laser, and (b) shows that the MIR seed laser is introduced in co-direction. (Solid line is blue laser output power, the dotted line is MIR output power).

results with MIR seed laser in co-direction case. When T is 160 °C, blue laser can be obtained after introducing of MIR seed laser, the maximum power is 0.231 W with length of 0.6 cm, which indicates that the introduction of MIR seed laser reduces the temperature threshold of TPAL system. When T is 180 ℃, 200 ℃ and 220 ℃, the maximum blue laser output powers in Fig7(a) are 0.022 W, 0.143 W and 0.575 W, corresponding to the optimal lengths of the cell are 0.75 cm, 0.7 cm and 0.6 cm, respectively. The maximum blue laser output powers in Fig7(b) are 1.274 W, 3.340 W and 6.604 W, the corresponding lengths of the cell are 0.55 cm, 0.5 cm, and 0.45 cm, respectively. The results show that for a certain T, there is an optimal L that maximizes P_{bout}. With MIR seed laser introducing and T increasing, the optimal vapor cell length decreases, and the corresponding P_{bout} increases. The explanation of the optimal L is that when the cell length is less than the optimal L, the pump laser cannot be fully absorbed so that the P_{bout} is lower. When the cell length exceeds the optimal L, the pump laser is completely absorbed at the front end of the alkali vapor cell, resulting that the Rb atoms in the back half of the vapor cell not being able to absorb enough pump laser to be excited, and Rb vapor forms an absorption loss on the blue laser, which results in the decrease of P_{bout}. The higher the T, the shorter the optimal L because Rb population densities increase with the T increase, and the L required to ensure complete absorption of the pump is shorter; therefore, the optimal L is shorter. After the introduction of MIR seed laser, the conversion efficiency of blue and MIR laser increases, which accelerates the absorption of pump laser, the optimal L required to ensure complete absorption of the pump laser is shorter, so the optimal length is shorter.

As for the MIR laser, Fig. 7(b) shows that when T is 160 °C, 180 °C, 200 °C and 220 °C, the maximum output powers of MIR laser can achieve 0.916 W, 1.122 W, 1.569 W, 2.358 W, respectively. As T increases, the concentration of Rb atoms increases, and the gain increases; thus, P_{rout} increases with enhancing in the working temperature. We also find that as the length of the vapor cell increases, the P_{rout} increases, and the trend of saturation gradually appears. Since the lower energy level of MIR laser is $6^2P_{3/2}$, it is easy to form particle number inversion, resulting in the gain of MIR laser can be achieved even if the pump intensity is weak.

For the single-wavelength pumped Rb-TPAL, high pump intensity is generally essential to promote the two-photon absorption process, and the pump threshold intensity is a key parameter. In order to investigate the pump thresholds of blue and MIR laser, P_{rin} is set to 0.1 W, and the other parameters were the same as mentioned above. Fig. 8 exhibits the dependence of the output power on the pump power at different temperatures with the optimal L. For the blue laser, Fig. 8(a) shows the Rb-TPAL system without MIR seed laser: when temperatures T is 180 ℃, 200 ℃ and 220 ℃, the pump threshold intensities are 1.413×10^4 W/cm^2, 1.393×10^4 W/cm^2 and 1.154×10^4 W/cm^2, respectively. Fig. 8(b) shows the Rb-TPAL system with MIR seed laser in the co-direction case: when temperatures T is 160 ℃, 180 ℃, 200 ℃ and 220 ℃, the corresponding pump threshold intensities of blue laser are 1.512×10^4 W/cm^2, 1.253×10^4 W/cm^2, 1.134×10^4 W/cm^2 and 1.054×10^4 W/cm^2, respectively. It can be seen that the MIR seed laser can reduce the pump and temperature thresholds of blue laser.

When T is 160 ℃, 180 ℃, 200 ℃ and 220 ℃, the threshold intensities of MIR laser are 6.167×10^3 W/cm^2, 3.581×10^3 W/cm^2, 2.586×10^3 W/cm^2 and 1.592×10^3 W/cm^2, respectively. The results show that the MIR laser threshold is much lower than the blue laser threshold. The reason is that the lower level of blue laser is the ground state, it requires strong pump intensity to form particle number inversion. However, the lower level of MIR laser is $6^2P_{3/2}$, which is an excited stated and basically empty at room temperature. It is easy to form particle number inversion between $5^2D_{5/2}$ and $6^2P_{3/2}$. Therefore, the generation of MIR laser is easier than the blue laser. The similar results have also been proved in the experiment [29]. The blue and MIR laser thresholds of pulse pumped Cs-TPAL were tested in Ref [29], and the values were 0.3 mJ and 3 nJ, respectively. The blue laser threshold was much higher than the MIR laser threshold, indicating that our calculation results agree with the experiment.

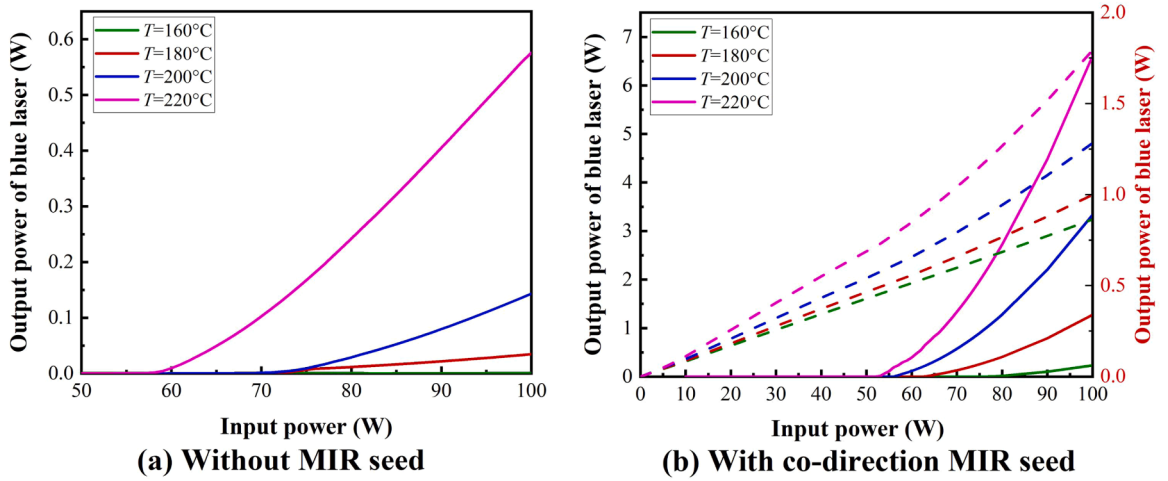

Fig. 8. Dependence of output power and input power at different temperatures when P_{rin}= 0.1 W. (a) is no introduced MIR seed laser, and (b) shows that the MIR seed laser is introduced in co-direction propagating with the blue laser (Solid line is blue laser output power, the dotted line is MIR output power).

3.3. Waist radii of pump and MIR seed laser

From the above simulation results, the temperature T is set to 220 °C, L is chosen to be 0.45 cm, the pump beam waist is located on the center of the vapor cell and the other parameters are the same as mentioned above. For the LD pumped TPALs with MIR seed, the pump beam waist radius w_p and MIR seed waist radius w_r have a significant effect on the output power. Therefore, we obtain the relationship between the output power and pump waist radius of MIR seed laser w_r at different pump waist radii w_p as shown in Fig. 9.

The Fig. 9 shows that when w_p is 300 μm, 400 μm,500 μm and 600 μm, and he Rayleigh lengths of the pump beam are 36.34 cm, 64.60 cm, 100.94 cm and 145.35 cm,corresponding to the output powers of blue laser are 12.680 W, 6.611 W, 2.453 W and 0.313 W, respectively. P_{bout} increases with the decrease of w_p. Because the pump laser intensity increases as w_p decreases, and more Rb atoms can be excited to $5^2D_{5/2}$ level and the gain increases, which causes the blue laser power increasing. However, w_r has little effect on P_{bout}. Fig. 10(a-c) illustrates the gain coefficients distribution of blue laser in the cell under steady state for a waist radius when wr is 300 μm, 400 μm and 500 μm, respectively. It can be seen that the gain of blue laser is almost unchanged under different w_r.

Fig. 9 also show that P_{rout} increases with the w_r increasing, This can be attributed to the distribution of the gain coefficients of MIR laser in the cell under steady state for w_r= 300 μm, 400 μm and 500 μm, as illustrated in Fig. 10(e-f). As w_r increases the MIR gain becomes larger, which lead to the increase of P_{rout}. Moreover, P_{rout} increases with the w_p decreasing. When w_p is 300 μm, 400 μm, 500 μm and 600 μm, the maximum MIR laser power with w_r of 500 μm can reach 4.940 W, 2.363 W, 1.520 W and 1.211 W, respectively. Because higher pump laser intensity can also improve the MIR laser power. The above results show that high-power blue and MIR laser output can be obtained by choosing smaller waist radius of pump laser and larger waist radius of MIR seed laser in the experiment.

3.4. Output mirror reflection

In this section, the value of w_r is chosen to be 500 μm. The other parameters are the same as above. We analyze the relationship between the output power and the blue laser reflectivity of the output mirror R_b at different pump waist radii w_p.

Fig. 11 displays that the output power as function of output mirror reflectance of blue laser when w_p are 300 μm, 400 μm,500 μm and 600 μm. When w_p are 300 μm and 400 μm, as R_b decreases, the P_{bout} increases. When $R_b = 0$, the blue laser power reaches the maximum, which is 13.587 W and 6.880 W, respectively. The results reveal that the Rb-TPAL system can obtain high-power blue laser output without the resonator cavity. When w_p are 500 μm and 600 μm, the optimal R_b are 5% and 30%, and the maximum output powers of blue laser are 2.471 W and 0.333 W, respectively. When $R_b = 0$, the output powers of blue laser are 2.432 W and 0.245 W, which indicates that high-power blue laser can also be obtained without resonant cavity. The results in Fig. 11 also show that P_{bout} increases with the decrease of w_p, which is consistent with the conclusion of Section 3.3.

From the Fig. 11, we can also see that R_b has little effect on the P_{rout}. When w_p are 300 μm, 400 μm,500 μm and 600 μm, output powers of MIR laser are ~5 W, ~2.4 W, ~1.5 W and ~1.2 W, respectively. It can be seen that high-power MIR laser output can be obtained even without resonant cavity. In experiment, since the resonant cavity mirror of TPAL system needs to consider the coating of blue laser, near-infrared laser and MIR laser, the technology is complex and the cost is high. Therefore, the resonant cavity can be eliminated in the experiment, and the adjustment of the resonant cavity can be avoided.

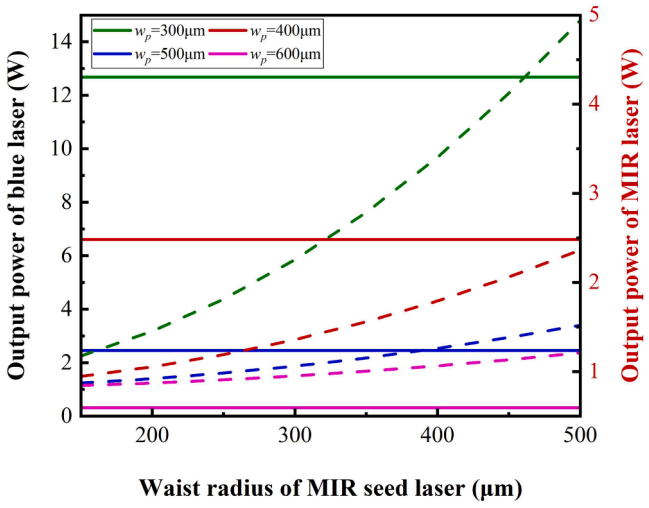

Fig. 9. Output power as function of waist radius of introduced MIR seed laser at different pump waist radii (Solid line is blue laser output power, the dotted line is MIR laser output power).

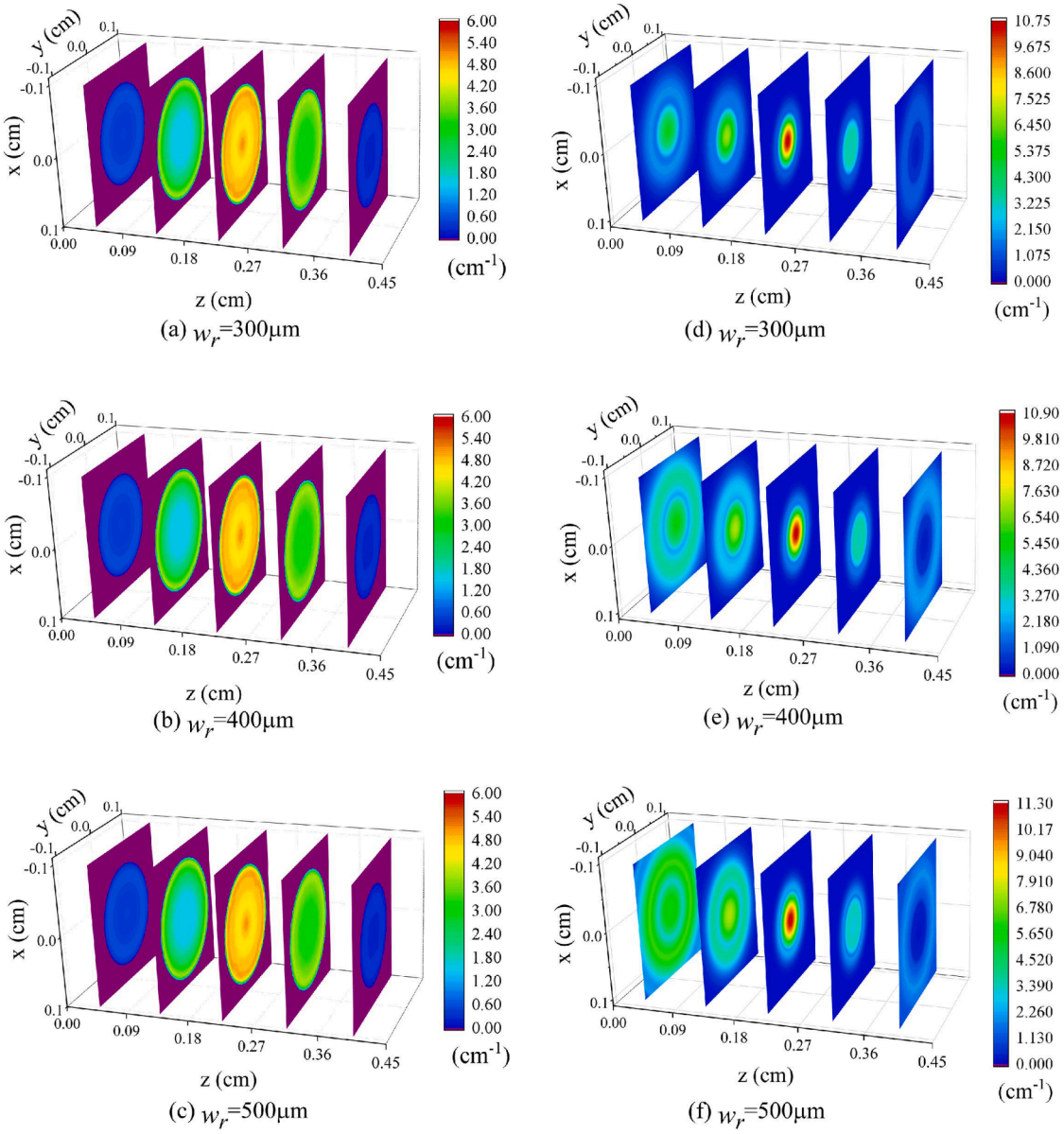

Fig. 10. Distribution of gain coefficients in the vapor cell at steady state under different waist w_r when w_p = 300 μm ((a-c) are gain coefficients of blue laser (d-f) are gain coefficients of MIR laser).

4. Conclusion

In this study, we establish a 3D single-wavelength CW TPAL theoretical model considering the MIR laser stimulated radiation and simulate the effect of MIR seed laser on the characteristics of Rb-TPAL for the first time. Firstly, we verify that the introduction of 5.23-μm MIR seed laser can significantly increase the output power and optical–optical conversion efficiency of blue laser, which verify the similar scheme in Ref. [25]. As for the direction of the MIR seed laser, Rb-TPAL in co-direction case has a simple structure and can obtain high-power coaxial and co-direction dual-band lasers, which is suitable for the Rb-TPAL system. For the vapor cell temperature and length, an optimal combination of temperature and cell length can maximize blue and MIR laser output power. With MIR seed laser and the increase of cell temperature, the corresponding optimal cell length decreases, and higher blue and MIR laser output powers are achieved. The pump and temperature thresholds of blue laser can also be reduced by introducing MIR seed. Moreover, the threshold of MIR laser is much lower than blue laser, which is consistent with the experimental results of Ref. [29]. As for the waist radii of pump and MIR seed, with the pump waist radius of the pump beam decreases, the output power of blue and MIR laser increase. With the MIR seed waist radius increasing, the MIR laser output power increases, but the output power of blue laser is almost unchanged. The high-power lasers output can be obtained without resonator cavity, which can simplify experimental device and save the

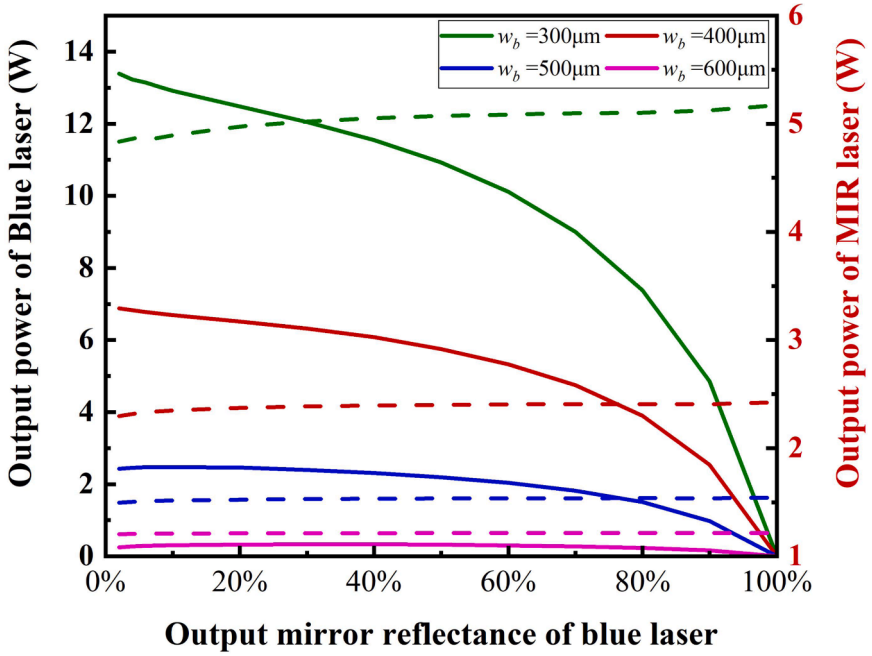

Fig. 11. Output power as function of output mirror reflectance of blue laser under different pump waist radii (Solid line is blue laser output power, the dotted line is MIR laser output power).

cost. This simulation results are very useful for designing TPAL system with high-power blue and MIR dual-band laser output.

CRediT authorship contribution statement

Yanhui Ji: Conceptualization, Methodology, Data curation, Formal analysis, Software, Writing – original draft. **Yang He**: Methodology, Software, Supervision, Writing – review & editing. **Li Pan**: Writing – review & editing. **Jiamin Wang**: Writing – review & editing. **Fei Chen**: Supervision, Writing – review & editing.

Declaration of Competing Interest

The authors declare that they have no known competing financial interests or personal relationships that could have appeared to influence the work reported in this paper.

Data availability

Data will be made available on request.

Acknowledgements

The authors want to acknowledge the support provided by 'National Natural Science Foundation of China' (61975203, 62005274), 'Open Fund Project of the State Key Laboratory of Laser and Material Interaction' (SKLLIM2012), 'Youth Innovation Promotion Association of CAS' (2022216).

References

[1] Y. Ji, Y. He, H. Wan, J. Wang, F. Chen, Theoretical modeling and analysis of blue laser characteristics of continuous-wave single-wavelength two-photon pumped Rb-vapor laser, IEEE J. Quantum Electron. 58 (2021) 1–8.
[2] D. Hostutler, Characterization of a Diode Pumped Alkali Laser with a Flowing Gain Medium, HPLS&A ConfGmunden, Austria, 2016.
[3] A.V. Bogachev, S.G. Garanin, A.M. Dudov, V.A. Eroshenko, S.M. Kulikov, G.T. Mikaelian, V.A. Panarin, V.O. Pautov, A.V. Rus, S.A. Sukharev, Diode-pumped caesium vapour laser with closed-cycle laser-active medium circulation, Quantum Electron. 42 (2012) 95–98.
[4] G.A. Pitz, D.M. Stalnaker, E.M. Guild, B.Q. Oliker, P.J. Moran, S.W. Townsend, D.A. Hostutler, Advancements in flowing diode pumped alkali lasers, in: S. J. Davis, M.C. Heaven, J.T. Schriempf (Eds.), High Energy/Average Power Lasers and Intense Beam Applications Ix, Spie-Int Soc Optical Engineering, Bellingham, 2016.
[5] M. Vlk, A. Datta, S. Alberti, H.D. Yallew, V. Mittal, G.S. Murugan, J. Jágerská, Applications, extraordinary evanescent field confinement waveguide sensor for mid-infrared trace gas spectroscopy, Light Sci. Appl. 10 (2021) 1–7.

[6] M.F. Ali, D.N.K. Jayakody, Y.A. Chursin, S. Affes, S. Dmitry, Recent advances and future directions on underwater wireless communications, Arch. Comput. Methods Eng. 27 (2020) 1379–1412.
[7] M. Yan, P.-L. Luo, K. Iwakuni, G. Millot, T.W. Hänsch, N. Picqué, Mid-infrared dual-comb spectroscopy with electro-optic modulators, Light. Sci. Appl. 6 (2017) e17076-e17076.
[8] Y. Du, C.-L. Zou, C. Zhang, K. Wang, C. Qiao, J. Yao, Y.S. Zhao, Tuneable red, green, and blue single-mode lasing in heterogeneously coupled organic spherical microcavities, Light. Sci. Appl. 9 (2020) 1–9.
[9] R. Roy, P.C. Condylis, Y.J. Johnathan, B. Hessmo, Atomic frequency reference at 1033 nm for ytterbium(Yb)-doped fiber lasers and applications exploiting a rubidium(Rb) 5S(1/2) to 4D(5/2) one- colour two-photon transition, Opt. Express 25 (2017) 7960–7969.
[10] N.D. Haluska, G.P. Perram, C.A. Rice, Efficient cascade lasing on over 17 wavelengths from two-photon excitation of the cesium 6(2)D states, Opt. Commun. 476 (2020).
[11] Y. Kato, B.J.J. Stoicheff, Two-photon absorption to highly excited D states of Rb atoms, 66 (1976) 490–492.
[12] F. Nez, F. Biraben, R. Felder, Y.J.Oc Millerioux, Optical frequency determination of the hyperfine components of the 5S12–5D32 two-photon transitions in rubidium, 102 (1993) 432–438.
[13] B.P. Stoicheff, E. Weinberger, Doppler-free two-photon absorption spectrum of rubidium, Can. J. Phys. 57 (1979) 2143–2154.
[14] T. Efthimiopoulos, M.E. Movsessian, M. Katharakis, N. Merlemis, Cascade emission and four wave mixing parametric processes in potassium, J. Appl. Phys. 80 (1996) 639–643.
[15] Y.C. Lee, Y.H. Chang, Y.Y. Chen, C.C. Tsai, H.C. Chui, Polarization and pressure effects in caesium 6S–8S two-photon spectroscopy, J. Phys. B At. Mol. Opt. Phys. 43 (2010) 235003–235008.
[16] H. Liu, J.-P. Yuan, L.-R. Wang, L.-T. Xiao, S.-T. Jia, Coherent 420 nm laser beam generated by four-wave mixing in Rb vapor with a single continuous-wave laser, Chin. Phys. B 29 (2020), 043203.
[17] N. Liu, S. Wang, J. Yuan, L. Wang, L. Xiao, S. Jia, Investigation of 6S 1/2–8S 1/2 two-photon transition of cesium atoms by a single 822 nm laser, Laser Phys. Lett. 19 (2022), 025201, 025205pp.
[18] N.D. Haluska, G.P. Perram, C.A. Rice, Efficient non-linear two-photon effects from the Cesium 6D manifold, Nonlinear Frequency Generation and Conversion: Materials and Devices XVII, International Society for Optics and Photonics (2018), 1051606.
[19] C. Rui, B. Gai, Y. Jie, L. Tong, J. Liu, H. Shu, J. Guo, Efficient generation of collimated frequency upconversion blue light in rubidium vapor, Chin. Opt. Lett. 013 (2015) 67–70.
[20] E. Brekke, S. Potier, Optical cavity for enhanced parametric four-wave mixing in rubidium, Appl. Opt. 56 (2017) 46–49.
[21] J. Yuan, H. Liu, L. Wang, L. Xiao, S. Jia, Coherent 420 nm light generated by the cavity-enhanced four-wave mixing process in Rb vapor, Opt. Express 29 (2021) 4858–4865.
[22] Y. Sebbag, Y. Barash, U. Levy, Generation of coherent mid-IR light by parametric four-wave mixing in alkali vapor, Opt. Lett. 44 (2019) 971.
[23] J.F. Sell, M.A. Gearba, B.D. Depaola, R.J. Knize, Collimated blue and infrared beams generated by two-photon excitation in Rb vapor, Opt. Lett. 39 (2014) 528–531.
[24] A.M. Akulshin, N. Rahaman, S.A. Suslov, R.J. McLean, Amplified spontaneous emission at 5.23 μm in two-photon excited rubidium vapor, J. Opt. Soc. Am. B 34 (2017) 2478–2484.
[25] B. Gai, R. Cao, X. Xia, S. Hu, J. Liu, J. Guo, Y. Tan, W. Liu, Y. Jin, F. Sang, Modulation of a double-line frequency up-conversion process in cesium vapor, Appl. Phys. B 122 (2016) 1–7.
[26] Z. Yang, H. Wang, Q. Lu, L. Liu, Y. Li, W. Hua, X. Xu, J. Chen, Theoretical model and novel numerical approach of a broadband optically pumped three-level alkali vapour laser, J. Phys. B At. Mol. Phys. 44 (2011), 085401.
[27] H. Yu, F. Chen, Y. He, S. Zhang, Q.-k Pan, D. Yu, J. Xie, Theoretical modeling and analysis on the absorption cross section of the two-photon excitation in Rb, Opt. Express 26 (2018) 17254–17263.
[28] H. Shu, M. Bass, Three-dimensional computer model for simulating realistic solid-state lasers, 46 (2007) 5687–5697.
[29] C.V. Sulham, G.A. Pitz, G.P. Perram, Blue and infrared stimulated emission from alkali vapors pumped through two-photon absorption, Appl. Phys. B 101 (2010) 57–63.